Adipocytes as Anticancer Drug Delivery Depot

Di Wen,[1,2,3] Jinqiang Wang,[1,2,3] George Van Den Driessche,[4] Qian Chen,[1,2,3] Yuqi Zhang,[1,2,3] Guojun Chen,[1,2,3] Hongjun Li,[1,2] Jennifer Soto,[1,2] Ming Liu,[5] Masao Ohashi,[6] Zejun Wang,[1,2] Peter Abdou,[1,2] Quanyin Hu,[1,2,3] Gianpietro Dotti,[7] Song Li,[1,2] Denis Fourches,[4] and Zhen Gu[1,2,3,8,*]

SUMMARY

Tumor-associated adipocytes promote tumor growth by providing energy and causing chronic inflammation. Here, we have exploited the lipid metabolism to engineer adipocytes that serve as a depot to deliver cancer therapeutics at the tumor site. Rumenic acid (RA), as an anticancer fatty acid, and a doxorubicin prodrug (pDox) with a reactive oxygen species (ROS)-cleavable linker, are encapsulated in adipocytes to deliver therapeutics in a tumor-specific bioresponsive manner. After intratumoral or postsurgical administration, lipolysis releases the RA and pDox that is activated by intracellular ROS-responsive conversion, subsequently promoting antitumor efficacy. Furthermore, downregulation of PD-L1 expression is observed in tumor cells, favoring the emergence of $CD4^+$ and $CD8^+$ T cell-mediated immune responses.

INTRODUCTION

Cancer cells are frequently surrounded by nonmalignant cells that support tumor development.[1] Tumor-associated adipocytes (TAAs) are present within the tumor microenvironment (TME) and are recognized to promote angiogenesis by secreting adipokines that include hormones, growth factors, and cytokines.[2] Adipokines contribute in recruiting immune cells that favor the generation of low-grade chronic inflammation[3] and abundance of reactive oxygen species (ROS) in the TME and tumor cells.[4,5] Growth factors, including vascular endothelial growth factor (VEGF), promote angiogenesis and tumor growth.[6] In the TME, fatty acids in lipid droplets from the adipocytes can also provide energy to cancer cells[7,8] through the fatty acid-binding protein 4 (FABP4) and tumor cell-induced lipolysis.[9] Moreover, recent studies indicate that interleukin-6 (IL-6) and leptin secreted by the adipocyte induce PD-L1 expression in cancer cells via activation of the JAK/Stat3 pathway.[10] A switch from white fat to brown fat caused by tumor cells[11] can also promote the direct expression of PD-L1 in adipocytes.[12] Therefore, targeting TAAs may be used to interrupt and eliminate a significant source of nutrients and immune protection for tumor cells.

Here, we have leveraged adipocytes as a drug delivery depot to achieve local and sustained release of chemotherapeutics within the TME (Figure 1A). A ROS-responsive doxorubicin prodrug (pDox) is synthesized (Figure 1B) and encapsulated into adipocytes together with rumenic acid (RA), an anticancer fatty acid,[13–16] which meanwhile enhances the loading capacity of pDox inside the adipocytes. pDox can be delivered to cancer cells via activation of the lipid metabolic pathway mediated by FABP4 (Figure 1C) without affecting their physiologic lipid accumulation (Figure 1E). Finally, downregulation of PD-L1 in tumor cells mediated by engineered adipocytes promotes the effector function of infiltrating T cells (Figure 1D).

Progress and Potential

The tumor microenvironment composed of nonmalignant cells often promotes tumor growth by providing growth factors and preventing the infiltration of tumor-killing immune cells. It could be valuable to leverage the therapeutic potential of the nonmalignant cells within the tumor microenvironment for anticancer treatment. In this work, the adipocytes have been engineered with the encapsulation of an anticancer fatty acid and a bioresponsive doxorubicin prodrug for chemotherapy and simultaneously inducing an immunogenic tumor phenotype. These Trojan horse-like injectable engineered adipocytes can serve as a drug-delivery depot for sustained drug release with suppressed primary tumor growth and postsurgical tumor recurrence. This adipocyte-mediated drug-delivery strategy expands the scope of cell therapy and could be extended for treating other diseases associated with lipid metabolism pathways.

RESULTS AND DISCUSSION

RA Reversed the Protumorigenic Role of TAAs

We co-cultured 3T3-L1 cell-differentiated adipocytes with different cancer cells in a transwell system. Normal adipocytes promoted the growth of tumor cells (Figures S1A–S1D). Furthermore, adipokine profiling of the co-culture supernatant showed high levels of resistin and VEGF, known to facilitate tumor cell growth and metastasis,[17] and lipocalin-2, known to drive brown fat activation in adipocytes[18] as well as lipolysis that provides energy to tumor cells (Figures S2 and S3). To reverse the protumorigenic role of TAAs, we first evaluated the *in vitro* toxicity of the anticancer RA (Figure S1E), also named 9*Z*,11*E*-conjugated linoleic acid, and encapsulated it into adipocytes, followed by co-culturing these engineered adipocytes with tumor cells in transwell assays. Adipocytes loaded with RA (RA@adipocytes) significantly inhibited the growth of B16F10 and E0771 cells compared with nontreated cancer cells (Figures S1F and S1G). Furthermore, we observed that RA@adipocytes inhibited the expression of PD-L1 in B16F10 cells (Figure S1H), and favorably modified the profile of adipokine secretion (Figures S2 and S3), suggesting that this strategy could be exploited to improve antitumor effects mediated by effector T cells. The mechanism studies indicated that the downregulated phosphorylation of the PD-L1 upstream regulators, including STAT3 and AKT,[19,20] contributed to the PD-L1 downregulation by RA@adipocytes (Figure S1I).

The antitumor effects of RA@adipocytes were evaluated by utilizing the B16F10 melanoma mouse model. TAAs were detected within the TME (Figure S4A), and intratumor injection of RA@adipocytes significantly delayed tumor growth (Figures 1F–1I and S4B) without evident toxicity (Figure S4C). Moreover, 2 days after the second injection of RA@adipocytes, we observed lower PD-L1 expression in tumor cells (Figures 1J and S4D), increased tumor-infiltrating $CD4^+$ and $CD8^+$ T cells (Figures 1K, 1L, and S4E) and reduced regulatory T cells (Tregs) (Figures 1M and S4F) compared with control treatments. RA@adipocyte-mediated tumor suppression was confirmed by the TUNEL assay (Figure 1N), while immunofluorescence staining of infiltrated $CD4^+$ and $CD8^+$ T cells further supported the transition to an immunogenic tumor phenotype (Figure 1O). The serum concentration of several cytokines was also determined, indicating significant downregulation of IL-6 and interferon-γ (Figure S4G), which might also contribute to the PD-L1 downregulation.[21] To further verify the immunomodulatory effect of RA@adipocyte to the TME, we performed CD4- and CD8-depletion studies. The anticancer effect of RA@adipocyte was significantly reversed after CD4 and CD8 depletion (Figure S5).

We further investigated the antitumor activity of RA@adipocytes in a tumor resection model. RA@adipocytes encapsulated into a fibrin gel and injected into the tumor resection cavity significantly delayed tumor recurrence and growth (Figures S6A–S6D) without evident toxicity (Figure S6E). In this model, we also observed decreased expression of PD-L1 in tumor cells (Figures S6F and S6J), increased tumor-infiltrating $CD4^+$ T cells (Figures S6G and S6K) and $CD8^+$ T cells (Figures S6H and S6K), and decreased Tregs (Figures S6I and S6L). These results were further confirmed by immunohistochemistry and immunofluorescence staining, showing enhanced tumor cell apoptosis (Figure S6M) and T cell infiltration (Figure S6N).

RA@adipocytes Loaded with Dox Prodrug Promoted Tumor Cell Death

To further improve the therapeutic index of RA@adipocytes, we synthesized a Dox prodrug by conjugating Dox to the oleic acid with a phenylboronic acid-based ROS-responsive linker (Figures S7–S13), which can be cleaved in the presence of

[1]Department of Bioengineering, University of California, Los Angeles, Los Angeles, CA 90095, USA

[2]Jonsson Comprehensive Cancer Center, California NanoSystems Institute, and Center for Minimally Invasive Therapeutics, University of California, Los Angeles, Los Angeles, CA 90095, USA

[3]Joint Department of Biomedical Engineering, University of North Carolina at Chapel Hill and North Carolina State University, Chapel Hill, NC 27599, USA

[4]Department of Chemistry, North Carolina State University, Raleigh, NC 27695, USA

[5]Department of Physics, North Carolina State University, Raleigh, NC 27695, USA

[6]Department of Chemical and Biomolecular Engineering, Department of Chemistry and Biochemistry, University of California, Los Angeles, Los Angeles, CA 90095, USA

[7]Department of Microbiology and Immunology, School of Medicine, University of North Carolina at Chapel Hill, Chapel Hill, NC 27599, USA

[8]Lead Contact

*Correspondence: guzhen@ucla.edu

https://doi.org/10.1016/j.matt.2019.08.007

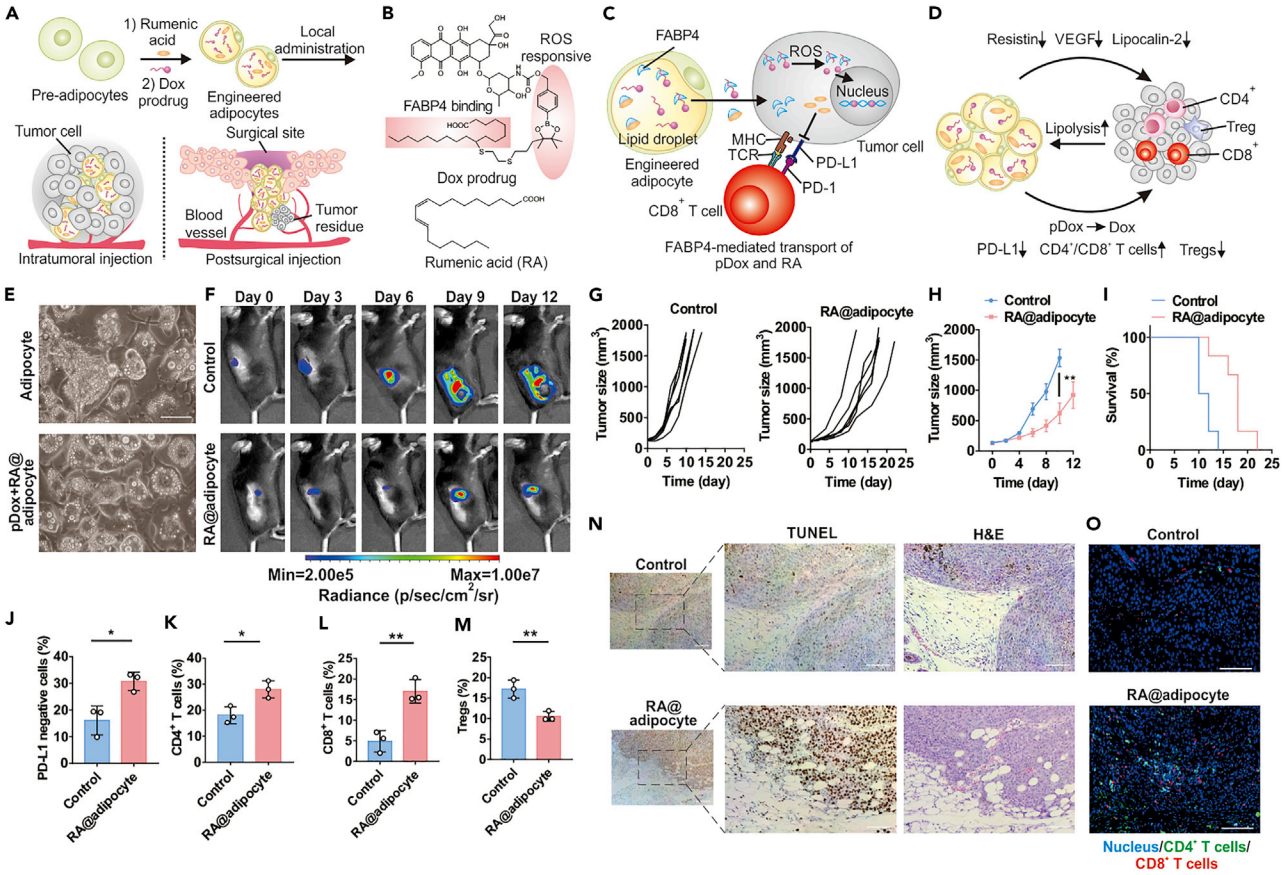

Figure 1. RA Reshapes the Protumorigenic Function of Adipocytes

(A–D) Schematic of the overall strategy. (A) pDox and RA were encapsulated into adipocytes and then inoculated intratumorally or within the tumor resection cavity. (B) Structure of the Dox prodrug (pDox) and RA. (C) Crosstalk between pDox + RA@adipocytes and tumor cells. (D) Therapeutic effect of pDox + RA@adipocytes. Figure S17.

(E–O) To evaluate the antitumor efficacy, 10^7 RA@adipocytes were injected intratumorally. (E) Representative figures (images from Figure S17A) of normally differentiated adipocytes and pDox + RA@adipocytes. Scale bar, 200 μm. (F) Representative figures (image from Figure S4B) of tumor bioluminescence in control or RA@adipocyte-treated mice. (G) Individual tumor growth kinetics of control and RA@adipocyte-treated mice. (H) Average tumor size in each experimental group. Data are presented as means ± SEM (n = 6). Statistical significance was calculated via Student's *t*-test. $p < 0.01$. (I) Survival curves of the mice in each group. (J–M) PD-L1-expressing tumor cells (J), $CD4^+$ T cells (K), $CD8^+$ T cells (L) and Tregs (M) within the tumor were quantified by flow cytometry. Data are presented as means ± SD (n = 3). Student's *t*-test was performed. *$p < 0.05$, **$p < 0.01$. (N and O) Tumor cell death (N; scale bars, 200 μm [left panel] and 100 μm [right panel]) and immune response (O; scale bar, 200 μm) caused by RA@adipocytes were evaluated by immunohistochemistry staining of TUNEL and immunofluorescence, respectively.

tumor-derived ROS.[22] Upon oxidation in 10 mM H_2O_2, pDox was converted to Dox within 48 h (Figure S14A). We hypothesized that the lipid conjugation in pDox would enhance the uptake of pDox by cancer cells through the lipid metabolic pathway. Binding of pDox and FABP4 was simulated (Figure 2A) and quantitatively characterized by the fluorescence polarization (Figures 2B and 2C). pDox had a high binding affinity to FABP4 (K_D = 23.1 nM), while there was almost no binding between Dox and FABP4. To simulate the binding interaction, we modified the structure of the linoleic acid and docked it into the FABP4 binding pocket (Figure S15A).[23,24] Furthermore, the ROS-responsive linker was constructed and conjugated to the lipid chain (Figure S15B). The pDox structure was generated using the Schrödinger Maestro's 3D-sketcher followed by an energy minimization procedure (Figure S15C) and a full-atom, 20-ns molecular dynamics simulation (Figure S16).[25] The binding affinity of lipids to FABP4 was significantly improved with the attached linker (Figures S15A and S15B). Dox attachment did not significantly alter the binding affinity of

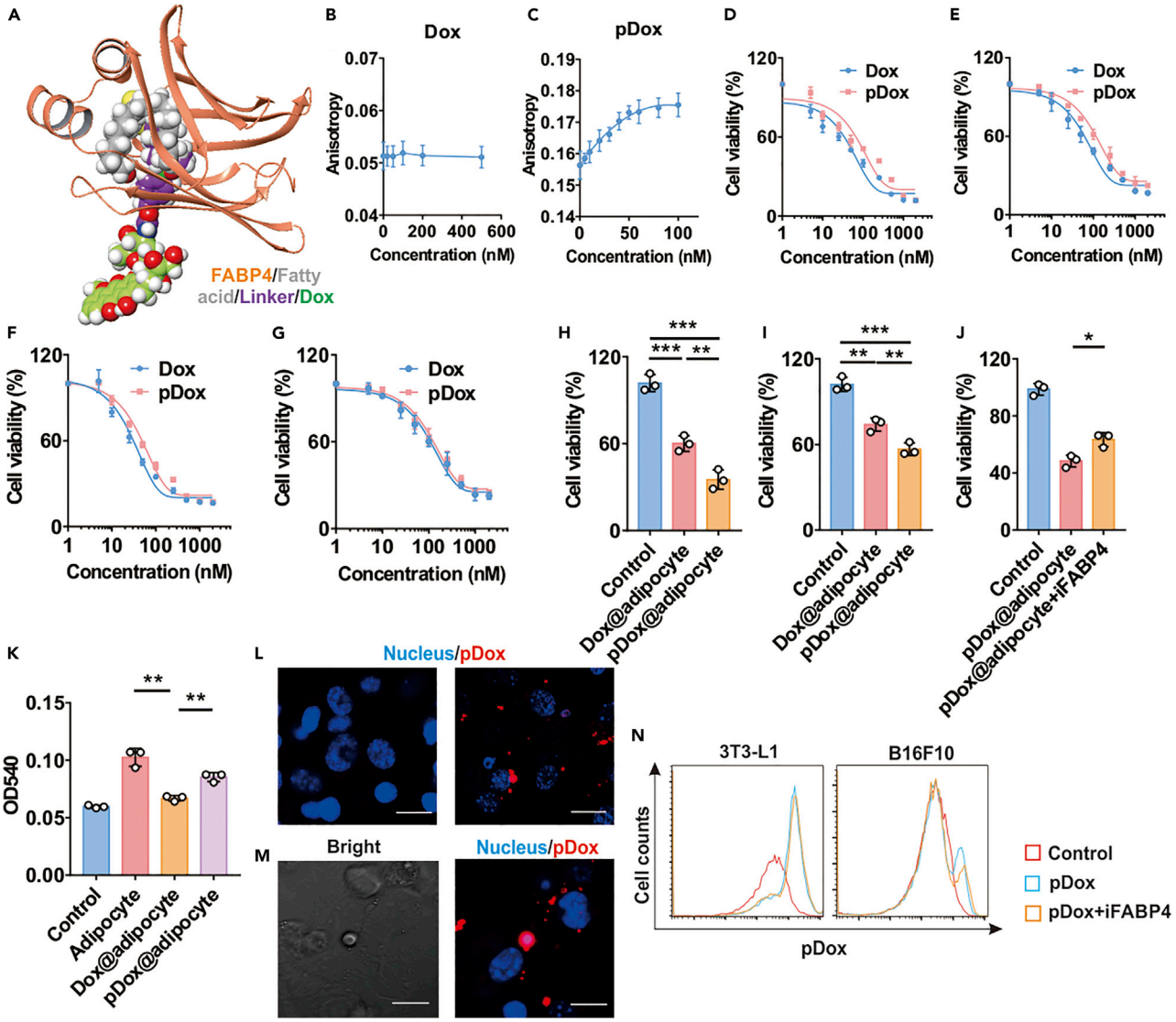

Figure 2. Characterization of the Doxorubicin Prodrug Loading into the Adipocytes

(A) Simulation of doxorubicin prodrug (pDox) and FABP4 binding.

(B and C) Binding affinity of Dox (B) and pDox (C) was determined by fluorescence polarization, n = 6.

(D–G) Cytotoxicity of pDox and Dox was determined in B16F10 (D), A375 (E), E0771 (F), and MCF-7 (G) cell lines, n = 3.

(H and I) pDox and Dox were further encapsulated into adipocytes and the antitumor effects were evaluated in B16F10 (H) and E0771 (I) cell lines. Data are presented as means ± SD (n = 3). Statistical significance was calculated via one-way ANOVA analysis with a Tukey post-hoc test. $^{**}p < 0.01$, $^{***}p < 0.001$.

(J) The effects of the FABP4 inhibitor were evaluated using the B16F10 cell line. Data are presented as means ± SD (n = 3). Statistical significance was calculated via one-way ANOVA analysis with a Tukey post-hoc test. $^{*}p < 0.05$.

(K) The inhibitory effects of Dox and pDox on lipid accumulation were determined by oil red O staining. Data are presented as means ± SD (n = 3). One-way ANOVA with a Tukey post hoc test was performed. $^{**}p < 0.01$.

(L and M) pDox encapsulation in adipocytes (Left panel: normally differentiated adipocytes. Right panel: pDox loaded adipocytes.) (L) and the intracellular localization of pDox (M) were determined by confocal fluorescence microscopy. Scale bars, 20 μm.

(N) Uptake of pDox in cancer cells was determined by flow cytometry after co-culturing B16F10 cells and pDox@adipocytes in a transwell assay.

the ligand, with Dox staying outside of the binding site, and pDox was indeed predicted to be a strong binder to FABP4 (Figure S15C). We also analyzed the dynamics of lipid (Video S1), lipid plus linker (Video S2), and pDox (Video S3), verifying their interactions with the FABP4 binding pocket.

Next, we assessed the cytotoxicity of pDox compared with Dox toward B16F10 (Figure 2D), A375 (Figure 2E), E0771 (Figure 2F), and MCF-7 (Figure 2G) cells. The IC_{50} of pDox toward B16F10, A375, and E0771 cells was about 1.5-fold higher than that of Dox. Dox and pDox were then added to 3T3-L1 cells to obtain Dox@adipocytes and pDox@adipocytes, respectively, which were then co-cultured with B16F10 (Figure 2H) and E0771 (Figure 2I) cells in a transwell assay. pDox@adipocytes showed enhanced cytotoxicity compared with Dox@adipocytes, and this effect was significantly reduced by BMS309403 that inhibits FABP4 (iFABP4) (Figure 2J). In accordance with a previous report,[26] Dox inhibited lipid accumulation in adipocytes (Figures 2K, S17A, and S17B). In addition, pDox could be efficiently encapsulated into adipocytes (Figure 2L) and accumulated in the lipid droplets (Figure 2M). During pDox absorption, iFABP4 did not affect the uptake of pDox in adipocytes. However, it significantly inhibited the transportation of pDox from adipocytes to B16F10 cells in the transwell assay (Figure 2N).

We further determined the antitumor effects of combining pDox and RA in B16F10 and E0771 cell lines (Figures 3A and 3B; combination index for B16F10 was 0.57). Both pDox and Dox were effectively loaded into RA@adipocytes (designated Dox + RA@adipocytes, pDox + RA@adipocytes) (Figure 3C) following the diffusion process,[27] while RA promoted the loading of both drugs (Figures S17C and S17D). The stability of pDox within RA@adipocyte was evaluated, indicating that pDox was not converted to Dox within 72 h (Figure S14B). The endosome was also labeled, indicating that pDox was preferentially localized in the lipid droplets (Figure S18A). We co-cultured pDox + RA@adipocytes and Dox + RA@adipocytes with B16F10 cells and used murine dermal fibroblasts as a control to compare drug-release profiles and lipolysis. B16F10 significantly triggered the release of Dox (Figure 3D) and pDox (Figure 3E) from adipocytes, while murine fibroblasts did not alter the release profile of both drugs. Furthermore, B16F10 induced lipolysis in adipocytes as indicated by the release of free fatty acids in the media, while fibroblasts did not trigger the lipid release (Figure 3F). However, more pDox tended to be accumulated in the lipid droplets compared with Dox, which exhibited a higher accumulation in the cell nucleus (Figure S18B). Therefore, more pDox was released from adipocytes compared with Dox after 72 h. The hydrogel formulated by fibrin did not affect the release profile of pDox within RA@adipocyte triggered by B16F10 (Figure S17E). In agreement with previous studies,[28,29] RA promoted lipid accumulation in the lipid droplets in 3T3-L1 cells (Figures 3G, 3I, S17A, and S17B). pDox + RA@adipocytes exhibited enhanced cytotoxicity to cancer cells compared with RA@adipocytes, and this effect was eliminated by blocking FABP4 (Figure 3H). In the same transwell system, RA encapsulation promoted pDox uptake in adipocytes and B16F10 cells, while the uptake of pDox by B16F10 was inhibited by iFABP4 (Figure 3J). The transportation of lipids from adipocytes to cancer cells was further confirmed by western blot (Figure S17F). Collectively, these data demonstrate that pDox can be effectively loaded into adipocytes and that pDox can be transferred to the tumor cells via lipid transportation and activation of lipolysis.

pDox + RA@adipocytes Promoted Chemotherapy- and Immunotherapy-Mediated Efficacy

To validate the therapeutic effects of pDox + RA@adipocytes *in vivo*, we utilized the B16F10 mouse melanoma model. pDox exhibited enhanced antitumor efficacy when delivered by adipocytes compared with free pDox loaded in the fibrin gel (Figures 4A, 4B, and S19A). Survival of mice receiving the pDox + RA@adipocytes was significantly enhanced (Figures 4C, S19A, and S19B) without evident toxicity (Figure S19C). When we analyzed the tumors collected 2 days after the second

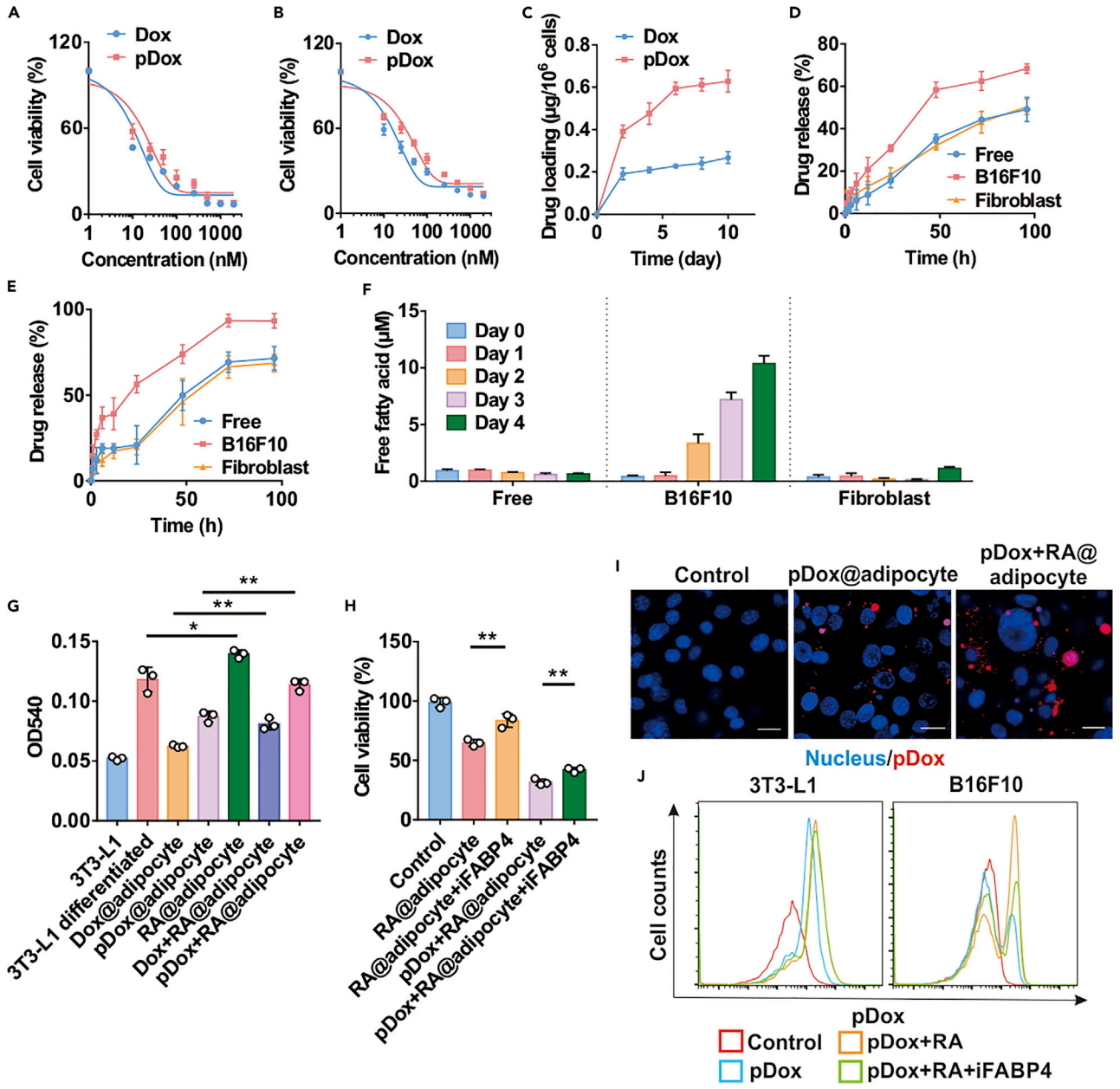

Figure 3. Combined RA and pDox Treatment for Cancer Therapy

(A and B) Antitumor effects of RA and Dox or pDox were determined in B16F10 (A) and E0771 (B) cell lines, n = 3.

(C) Comparison of the loading capacity of Dox and pDox in RA@adipocytes, n = 3.

(D–F) Release profile of Dox (D) and pDox (E) from adipocytes and concentration of free fatty acid (F) were determined in a transwell assay, n = 3.

(G) Lipid accumulation in adipocytes was evaluated by oil red O staining, n = 3.

(H) Cytotoxicity of pDox + RA@adipocytes in a transwell assay was determined by MTT assay. Data are presented as means ± SD (n = 3). One-way ANOVA with a Tukey post hoc test was performed. *$p < 0.05$, **$p < 0.01$.

(I) RA-loading capacity was determined using a confocal fluorescence microscope. Scale bars, 20 μm.

(J) pDox transportation between B16F10 cells and adipocytes mediated by FABP4 was determined by flow cytometry in a transwell assay.

treatment, mice treated with normally differentiated adipocytes exhibited slightly enhanced expression of PD-L1 in tumor cells (Figures 4D and S20A). We also observed decreased PD-L1 expression in tumor cells (Figures 4D and S20A),

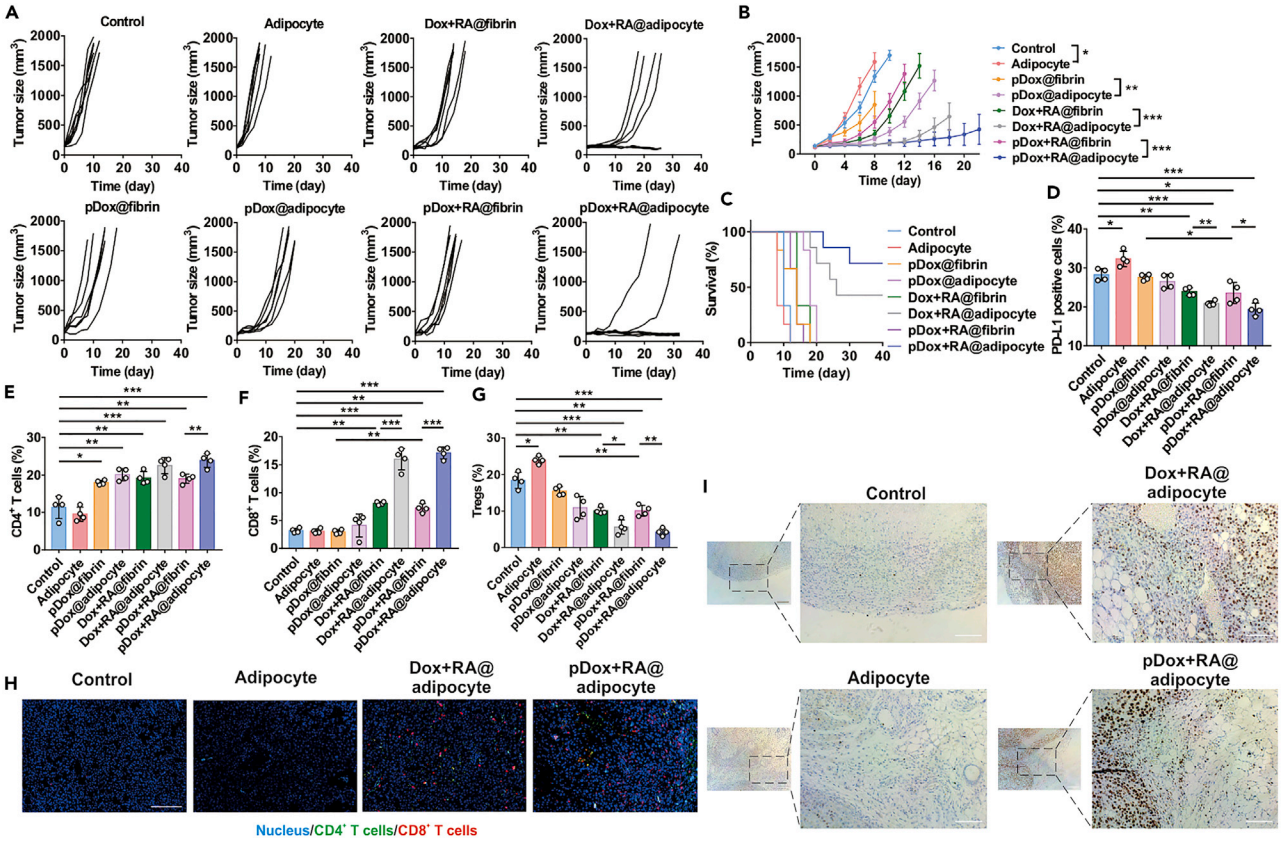

Figure 4. Drug-Loaded Adipocytes Suppress Tumor Growth

(A) Individual tumor growth kinetics.

(B) Average tumor size in each experimental group. Data are presented as means ± SEM (n = 6–7). One-way ANOVA with a Tukey post-hoc test was used for the analysis. *$p < 0.05$, **$p < 0.01$, ***$p < 0.001$.

(C) Survival curves of the mice in each group.

(D–G) PD-L1-expressing cells (D), $CD4^+$ T cells (E), $CD8^+$ T cells (F), and Tregs (G) were quantified within the tumor by flow cytometry. Data are presented as means ± SD (n = 4). One-way ANOVA with a Tukey post hoc test was performed. *$p < 0.05$, **$p < 0.01$, ***$p < 0.001$.

(H and I) Intratumor immune response (H; image from Figure S20D; scale bar, 200 μm) and tumor cell death of Dox + RA@adipocytes and pDox + RA@adipocytes (I; image from Figure S21; scale bars, 200 μm [left panel] and 100 μm [right panel]) were evaluated by immunofluorescence staining of T cells and immunohistochemistry TUNEL staining.

increased tumor-infiltrating $CD4^+$ T cells (Figures 4E and S20B) and $CD8^+$ T cells (Figures 4F and S20B), and reduced Tregs infiltration (Figures 4G and S20C) after pDox + RA@adipocyte treatment. These results were confirmed by immunofluorescence and immunohistochemistry staining showing enhanced T cell infiltration (Figures 4H and S20D) and tumor cell apoptosis (Figures 4I and S21). pDox + RA@adipocytes also protected mice from tumor recurrence in a tumor resection model (Figure S22A). Dox + RA@adipocytes and pDox + RA@adipocytes protected mice from tumor recurrence compared with control treatments (62.5% and 37.5%, respectively) (Figures S22B–S22D). Enhanced tumor cell death was achieved in Dox + RA@adipocytes and pDox + RA@adipocytes groups (Figure S24) without detectable toxicity (Figures S22E and S25). Of note, fibrin-loaded RA-treated groups exhibited significantly decreased PD-L1 expression in tumor cells, whereas RA-loaded adipocytes showed enhanced outcomes (Figures S22F and S23A). Meanwhile, the frequencies of $CD4^+$ (Figures S22G and S23B) and $CD8^+$ T cells (Figures S22H and S23B) were significantly enhanced, while a significant decrease of the

Treg population was observed (Figures S22I and S23C). These results were further confirmed by immunofluorescence staining, showing enhanced T cell infiltration (Figure S23D), especially in Dox + RA@adipocytes and pDox + RA@adipocytes groups.

Recent decades have witnessed fast development of cell therapy using cells or cell-derived particles as drug delivery systems due to their unique transport process and intrinsic properties that facilitate drug delivery.[30] These drug delivery platforms, including erythrocytes,[31–33] platelets,[34–36] and stem cells,[37,38] are mainly administered intravenously due to their long circulation or targeting capabilities to the tumor or inflammatory sites. For solid tumors, surgical resection of primary tumors combined with chemotherapy, radiotherapy, or immunotherapy remains the main option.[39] The local drug delivery depot with high biocompatibility to the TME is highly desired for clinical applications. Adipocytes are widely present in the human body, and the procedures including isolation, purification, and differentiation of preadipocytes are straightforward and robust. In addition, the lipid droplets accumulated in adipocytes are natural carriers for hydrophobic drugs. The lipolysis triggered by tumor cells can modulate the drug release profile in a TME-associated metabolism-responsive manner. Genetically engineered adipocytes may further serve as therapeutic depots with desired adipokines and/or membrane proteins.

In summary, the protumorigenic role of adipocytes can be reverted through "lipid cargo engineering" with integration of anticancer lipid molecules. Antitumor effects mediated by TAAs can be achieved by localized drug delivery to tumor cells exploiting the FABP4-mediated lipid transportation. Furthermore, RA@adipocytes induced an immunogenic tumor phenotype by downregulating PD-L1 expression, allowing infiltration of effector T cells. This adipocyte-mediated drug delivery strategy could be extended to treat a variety of diseases involving the lipid metabolisms.

EXPERIMENTAL PROCEDURES

Materials

All chemicals were purchased from Sigma-Aldrich and used as received unless otherwise specified. Doxorubicin hydrochloride was purchased from Oakwood Chemical. BMS309403, the FABP4 inhibitor, was purchased from Cayman Chemical. RA (9Z, 11E-CLA) (catalog no. 16413) was purchased from Sigma-Aldrich.

Cell Culture

Cell lines of 3T3-L1 (CL-173), B16F10 (CRL-6475), A375 (CRL-1619), and MCF-7 (HTB-22), were purchased from the American Type Culture Collection. E0771 cell line (940001) was purchased from CH3 Biosystems. Bioluminescent B16F10 cells (B16F10-luc-GFP) were provided by Dr. Leaf Huang from University of North Carolina at Chapel Hill. B16F10, A375, and MCF-7 cells were cultured in DMEM (Gibco, Invitrogen) with 10% fetal bovine serum (FBS) (Gibco). E0771 cells were cultured in RPMI 1640 medium with 10% FBS and 10 mM HEPES (Thermo Fisher Scientific). Mouse primary dermal fibroblast was purchased from Cell Biologics (catalog no. C57-6067) and cultured using Fibroblast Medium Kit (catalog no. M2267). For culturing 3T3-L1, DMEM with 10% bovine calf serum (Thermo Fisher Scientific) was used as the medium. A 3T3-L1 Differentiation Kit (Sigma-Aldrich catalog no. DIF001) was used to differentiate 3T3-L1 preadipocytes. To achieve the maximum loading capacity, we used 10–20 passages of 3T3-L1 cells in this study.

Fluorescent Polarization

To determine the binding affinity of Dox or pDox to FABP4, we diluted all samples in phosphate buffered saline (PBS). Serial dilutions of FABP4 were added to Dox or pDox. Fluorescence polarization was measured using a QuantaMaster 40 UV/VIS Steady State Spectrofluorometer (Photon Technology International). The dissociation constant (K_D) was calculated for each by fitting the observed polarization to a general equation for two-state binding as previously described.[40]

Loading and Release of Dox, pDox, and RA

For generating RA- and Dox-loaded or pDox-loaded adipocytes, RA (200 μM) and Dox or pDox (500 nM) were added to the maintenance medium (DMEM/F12 [1:1] with 10% FBS and 1.5 mg/mL insulin) and changed every 48 h. Lipid accumulation in adipocytes was evaluated by oil red O staining and quantified by optical density measurement at 540 nm. Preadipocytes were cultured, differentiated, and encapsulated with drugs in 6-well transwell insert, and co-cultured with 5×10^5 pre-cultured B16F10 or fibroblasts in 6-well plates to determine drug-release profiles, which was calculated according to drug amount remained in adipocytes. The concentration of free fatty acid in the co-cultured medium was measured using a Free Fatty Acid Quantitation Kit (Sigma-Aldrich, catalog no. MAK044). To measure the amount of Dox and pDox in RA-loaded adipocytes, we added 20 μL of Triton X-100 to 10^6 adipocytes, then added 100 μL of extraction solution (0.75 M HCl in isopropanol) and incubated the mixture at −20°C overnight. The fluorescence of supernatant at 498 (excitation)/591 (emission) nm was measured after centrifugation at 20,000 × *g* for 15 min.[41] The maintenance medium containing drugs was changed three to four times before animal studies. A high-performance liquid chromatography method for Dox was used to determine the stability of pDox: an Agilent C18 column (4.6 × 50 mm) eluted with water and acetonitrile (starting at 95:5 and then after 15-min gradient up to 5:95).

Crosstalk between Cancer Cells and Adipocytes

Cytotoxicity of drug and fatty acid was determined by MTT assay in 96-well plate after 48 h. The tumor cell-killing or -promoting effect of drug- or fatty acid-loaded adipocytes was determined in a transwell system where adipocytes were seeded in the 24 well plate and tumor cells grew in the transwell insert.[42] After culturing for 72 h, cell proliferation of cancer cells in the transwell insert was determined by MTT assay.

For western blot, flow cytometry, and adipokine profiling (R&D Systems catalog no. ARY013), a 6-well transwell system was used with cancer cells cultured in the transwell insert and adipocytes in the bottom. Cells or medium were analyzed after co-culturing for 72 h. To determine the role of FABP4 during the crosstalk, we added 30 μM BMS309403 to the medium to block FABP4. Antibodies used for western blot included β-actin (catalog no. sc-47778, Santa Cruz Biotechnology), FABP4 (catalog no. 701158, Thermo Fisher), and PD-L1 (catalog no. ab205921, Abcam). The phycoerythrin channel was used to determine pDox fluorescence in adipocytes and cancer cells.

In Vivo Tumor Studies

For a subcutaneous model, 1×10^6 luciferase-tagged B16F10 cells were injected into the right flank of mice. When the tumor reached 50–100 mm^3, mice were randomly divided into different groups with intratumorally injected different formulations on day 0 and day 3, including fibrin gels, pDox-loaded fibrin gels, Dox- and RA-loaded fibrin gels, pDox- and RA-loaded fibrin gels, normally differentiated adipocytes, pDox-loaded adipocytes, Dox- and RA-loaded adipocytes, and pDox- and

RA-loaded adipocytes. The doses of Dox was 0.1 mg/kg (7–10 × 10^6 adipocytes). Tumor size was measured with a digital caliper and monitored by bioluminescence signal using an IVIS Lumina imaging system (PerkinElmer) with intraperitoneal injection of luciferin (catalog no. LUCK-100, Gold Biotechnology) at 150 mg/kg. Tumor volume was calculated as long diameter × short diameter^2/2.

For a postsurgical recurrence model, 1 × 10^6 luciferase-expressed B16F10 cells were subcutaneously injected in the right flank of mice. When tumor size reached 200–300 mm^3, most tumor was resected, leaving about 1% residual tissue behind as previously reported.[43,44] The amount of residual tumor was determined by bioluminescence signal of B16F10 cells before and after surgery. The wound was closed by an Autoclip wound-clip system. After randomly dividing the mice into different groups, drugs or drug-loaded adipocytes were encapsulated into fibrin gels and further implanted into the surgical bed. Tumor growth was monitored by detecting the bioluminescence and measuring tumor size after removing the clips. For both intratumoral and postsurgical models, mice were euthanized when the tumor size exceeded 1.5 cm^3.

To determine the expression of PD-L1 in tumor cells and the population of T cells, we sacrificed four mice in each group to obtain the tumors 2 days after the second injection of formulation for intratumoral model. The same time point was utilized to determine the cytokine levels in blood serum. For the tumor recurrence model, tumors were harvested 1 week after surgery. A single-cell suspension of tumor was prepared using staining buffer (catalog no. 420201, BioLegend). A total of 20,000 events per sample were collected and analyzed using FlowJo software. Tumor sections were further analyzed by immunohistochemistry staining of hematoxylin and eosin, and immunofluorescence staining. Antibodies for detecting PD-L1-positive cells, $CD4^+$ T cells, $CD8^+$ T cells, and Tregs included CD3 (catalog no. 100203, Biolegend), CD4 (catalog no. 100515, Biolegend), CD8 (catalog no. 100707, Biolegend), PD-L1 (catalog no. 124311, Biolegend), and FoxP3 (catalog no. 126403, Biolegend).

Statistics

Student's *t*-test, one-way ANOVA and a Tukey post hoc test were performed for multiple comparisons. Data are presented as means ± SD or means ± SEM as noted in the figure legends. All tests were performed using the software GraphPad Prism. Significance is denoted in the figures as *$p < 0.05$, **$p < 0.01$, ***$p < 0.001$, and ****$p < 0.0001$.

SUPPLEMENTAL INFORMATION

Supplemental Information can be found online at https://doi.org/10.1016/j.matt.2019.08.007.

ACKNOWLEDGMENTS

This work was supported by grants from the start-up packages of UCLA and UNC/NC State, Sloan Research Fellowship of the Alfred P. Sloan Foundation, and Jonsson Comprehensive Cancer Center at UCLA. We thank Dr. Leaf Huang from University of North Carolina at Chapel Hill for providing Bioluminescent B16F10 cells.

AUTHOR CONTRIBUTIONS

D.W. and Z.G. were responsible for conception and experimental strategy of the study. D.W., J.W., G.V.D.D., Q.C., H.L., M.L., M.O., Z.W., and P.A. performed the

experiments and acquired the data. D.W., J.W., G.V.D.D., Q.C., Y.Z., G.C., H.L., J.S., M.L., M.O., Z.W., Q.H., G.D., S.L., D.F., and Z.G. interpreted the data and drafted the manuscript. Y.Z., G.C., G.D., and Q.H. supported the revision of the manuscript.

DECLARATION OF INTERESTS

Z.G. and D.W. have applied for patents related to this study. Z.G. is a scientific co-founder of ZenCapsule Inc. The other authors declare no competing interests.

Received: April 22, 2019
Revised: July 9, 2019
Accepted: August 8, 2019
Published: September 25, 2019

REFERENCES

1. Hanahan, D., and Weinberg, R.A. (2011). Hallmarks of cancer: the next generation. Cell *144*, 646–674.

2. Santander, A.M., Lopez-Ocejo, O., Casas, O., Agostini, T., Sanchez, L., Lamas-Basulto, E., Carrio, R., Cleary, M.P., Gonzalez-Perez, R.R., and Torroella-Kouri, M. (2015). Paracrine interactions between adipocytes and tumor cells recruit and modify macrophages to the mammary tumor microenvironment: the role of obesity and inflammation in breast adipose tissue. Cancers (Basel) *7*, 143–178.

3. Correa, L.H., Correa, R., Farinasso, C.M., de Sant'Ana Dourado, L.P., and Magalhaes, K.G. (2017). Adipocytes and macrophages interplay in the orchestration of tumor microenvironment: new implications in cancer progression. Front. Immunol. *8*, 1129.

4. Nieman, K.M., Romero, I.L., Van Houten, B., and Lengyel, E. (2013). Adipose tissue and adipocytes support tumorigenesis and metastasis. Biochim. Biophys. Acta *1831*, 1533–1541.

5. Liou, G.Y., and Storz, P. (2010). Reactive oxygen species in cancer. Free Radic. Res. *44*, 479–496.

6. Cao, Y. (2013). Angiogenesis and vascular functions in modulation of obesity, adipose metabolism, and insulin sensitivity. Cell Metab. *18*, 478–489.

7. Zhang, M., Di Martino, J.S., Bowman, R.L., Campbell, N.R., Baksh, S.C., Simon-Vermot, T., Kim, I.S., Haldeman, P., Mondal, C., Yong-Gonzales, V., et al. (2018). Adipocyte-derived lipids mediate melanoma progression via FATP proteins. Cancer Discov. *8*, 1006–1025.

8. Miranda, F., Mannion, D., Liu, S., Zheng, Y., Mangala, L.S., Redondo, C., Herrero-Gonzalez, S., Xu, R., Taylor, C., Chedom, D.F., et al. (2016). Salt-inducible kinase 2 couples ovarian cancer cell metabolism with survival at the adipocyte-rich metastatic niche. Cancer Cell *30*, 273–289.

9. Nieman, K.M., Kenny, H.A., Penicka, C.V., Ladanyi, A., Buell-Gutbrod, R., Zillhardt, M.R., Romero, I.L., Carey, M.S., Mills, G.B., Hotamisligil, G.S., et al. (2011). Adipocytes promote ovarian cancer metastasis and provide energy for rapid tumor growth. Nat. Med. *17*, 1498–1503.

10. Xu, L., Shen, M., Chen, X., Zhu, R., Yang, D.R., Tsai, Y., Keng, P.C., Chen, Y., and Lee, S.O. (2018). Adipocytes affect castration-resistant prostate cancer cells to develop the resistance to cytotoxic action of NK cells with alterations of PD-L1/NKG2D ligand levels in tumor cells. Prostate *78*, 353–364.

11. Petruzzelli, M., Schweiger, M., Schreiber, R., Campos-Olivas, R., Tsoli, M., Allen, J., Swarbrick, M., Rose-John, S., Rincon, M., Robertson, G., et al. (2014). A switch from white to brown fat increases energy expenditure in cancer-associated cachexia. Cell Metab. *20*, 433–447.

12. Ingram, J.R., Dougan, M., Rashidian, M., Knoll, M., Keliher, E.J., Garrett, S., Garforth, S., Blomberg, O.S., Espinosa, C., Bhan, A., et al. (2017). PD-L1 is an activation-independent marker of brown adipocytes. Nat. Commun. *8*, 647.

13. Tanmahasamut, P., Liu, J., Hendry, L.B., and Sidell, N. (2004). Conjugated linoleic acid blocks estrogen signaling in human breast cancer cells. J. Nutr. *134*, 674–680.

14. Arab, A., Akbarian, S.A., Ghiyasvand, R., and Miraghajani, M. (2016). The effects of conjugated linoleic acids on breast cancer: a systematic review. Adv. Biomed. Res. *5*, 115.

15. Lu, G., Zhang, G., Zheng, X., Zeng, Y., Xu, Z., Zeng, W., and Wang, K. (2015). C9, t11-conjugated linoleic acid induces HCC cell apoptosis and correlation with PPAR-gamma signaling pathway. Am. J. Transl. Res. *7*, 2752–2763.

16. Ochoa, J.J., Farquharson, A.J., Grant, I., Moffat, L.E., Heys, S.D., and Wahle, K.W. (2004). Conjugated linoleic acids (CLAs) decrease prostate cancer cell proliferation: different molecular mechanisms for cis-9, trans-11 and trans-10, cis-12 isomers. Carcinogenesis *25*, 1185–1191.

17. Pang, L., Zhang, Y., Yu, Y., and Zhang, S. (2013). Resistin promotes the expression of vascular endothelial growth factor in ovary carcinoma cells. Int. J. Mol. Sci. *14*, 9751–9766.

18. Zhang, Y., Guo, H., Deis, J.A., Mashek, M.G., Zhao, M., Ariyakumar, D., Armien, A.G., Bernlohr, D.A., Mashek, D.G., and Chen, X. (2014). Lipocalin 2 regulates brown fat activation via a nonadrenergic activation mechanism. J. Biol. Chem. *289*, 22063–22077.

19. Song, T.L., Nairismagi, M.L., Laurensia, Y., Lim, J.Q., Tan, J., Li, Z.M., Pang, W.L., Kizhakeyil, A., Wijaya, G.C., Huang, D.C., et al. (2018). Oncogenic activation of the STAT3 pathway drives PD-L1 expression in natural killer/T-cell lymphoma. Blood *132*, 1146–1158.

20. Lastwika, K.J., Wilson, W., 3rd, Li, Q.K., Norris, J., Xu, H., Ghazarian, S.R., Kitagawa, H., Kawabata, S., Taube, J.M., Yao, S., et al. (2016). Control of PD-L1 expression by oncogenic activation of the AKT-mTOR pathway in non-small cell lung cancer. Cancer Res. *76*, 227–238.

21. Garcia-Diaz, A., Shin, D.S., Moreno, B.H., Saco, J., Escuin-Ordinas, H., Rodriguez, G.A., Zaretsky, J.M., Sun, L., Hugo, W., Wang, X., et al. (2017). Interferon receptor signaling pathways regulating PD-L1 and PD-L2 expression. Cell Rep. *19*, 1189–1201.

22. Lu, Y., Aimetti, A.A., Langer, R., and Gu, Z. (2016). Bioresponsive materials. Nat. Rev. Mater. *1*, 16075.

23. Friesner, R.A., Banks, J.L., Murphy, R.B., Halgren, T.A., Klicic, J.J., Mainz, D.T., Repasky, M.P., Knoll, E.H., Shelley, M., Perry, J.K., et al. (2004). Glide: a new approach for rapid, accurate docking and scoring. 1. method and assessment of docking accuracy. J. Med. Chem. *47*, 1739–1749.

24. Halgren, T.A., Murphy, R.B., Friesner, R.A., Beard, H.S., Frye, L.L., Pollard, W.T., and Banks, J.L. (2004). Glide: a new approach for rapid, accurate docking and scoring. 2. Enrichment factors in database screening. J. Med. Chem. *47*, 1750–1759.

25. Guo, Z., Mohanty, U., Noehre, J., Sawyer, T.K., Sherman, W., and Krilov, G. (2010). Probing the alpha-helical structural stability of stapled p53 peptides: molecular dynamics simulations and analysis. Chem. Biol. Drug Des. *75*, 348–359.

26. Biondo, L.A., Lima Junior, E.A., Souza, C.O., Cruz, M.M., Cunha, R.D., Alonso-Vale, M.I., Oyama, L.M., Nascimento, C.M., Pimentel, G.D., Dos Santos, R.V., et al. (2016). Impact of doxorubicin treatment on the physiological functions of white adipose tissue. PLoS One *11*, e0151548.

27. Thompson, B.R., Lobo, S., and Bernlohr, D.A. (2010). Fatty acid flux in adipocytes: the in's and out's of fat cell lipid trafficking. Mol. Cell. Endocrinol. *318*, 24–33.

28. Sakuma, S., Nishioka, Y., Imanishi, R., Nishikawa, K., Sakamoto, H., Fujisawa, J., Wada, K., Kamisaki, Y., and Fujimoto, Y. (2010). Cis9, trans11-conjugated linoleic acid differentiates mouse 3T3-L1 preadipocytes into mature small adipocytes through induction of peroxisome proliferator-activated receptor gamma. J. Clin. Biochem. Nutr. *47*, 167–173.

29. den Hartigh, L.J., Han, C.Y., Wang, S., Omer, M., and Chait, A. (2013). 10E,12Z-conjugated linoleic acid impairs adipocyte triglyceride storage by enhancing fatty acid oxidation, lipolysis, and mitochondrial reactive oxygen species. J. Lipid Res. *54*, 2964–2978.

30. Chen, Z., Wang, Z., and Gu, Z. (2019). Bioinspired and biomimetic nanomedicines. Acc. Chem. Res. *52*, 1255–1264.

31. Wang, C., Ye, Y., Sun, W., Yu, J., Wang, J., Lawrence, D.S., Buse, J.B., and Gu, Z. (2017). Red blood cells for glucose-responsive insulin delivery. Adv. Mater. *29*, https://doi.org/10.1002/adma.201606617.

32. Hu, C., Zhang, L., Aryal, S., Cheung, C., Fang, R., and Zhang, L. (2011). Erythrocyte membrane-camouflaged polymeric nanoparticles as a biomimetic delivery platform. Proceedings of the National Academy of Sciences of the United States of America *108*, 10980–10985.

33. Yan, J., Yu, J., Wang, C., and Gu, Z. (2017). Red blood cells for drug delivery. Small Methods *1*, 1700270.

34. Hu, Q., Sun, W., Qian, C., Wang, C., Bomba, H.N., and Gu, Z. (2015). Anticancer platelet-mimicking nanovehicles. Adv. Mater. *27*, 7043–7050.

35. Lu, Y., Hu, Q., Jiang, C., and Gu, Z. (2018). Platelet for drug delivery. Curr. Opin. Biotechnol. *58*, 81–91.

36. Wang, C., Sun, W., Ye, Y., Bomba, H., and Gu, Z. (2017). *In situ* activation of platelets with checkpoint inhibitors for post-surgical cancer immunotherapy. Nature Biomedical Engineering *1*, 0011.

37. Hu, Q., Sun, W., Wang, J., Ruan, H., Zhang, X., Ye, Y., Shen, S., Wang, C., Lu, W., Cheng, K., et al. (2018). Conjugation of haematopoietic stem cells and platelets decorated with anti-PD-1 antibodies augments anti-leukaemia efficacy. Nat. Biomed. Eng. *2*, 831–840.

38. Tang, J., Su, T., Huang, K., Dinh, P.U., Wang, Z., Vandergriff, A., Hensley, M.T., Cores, J., Allen, T., Li, T., et al. (2018). Targeted repair of heart injury by stem cells fused with platelet nanovesicles. Nat. Biomed. Eng. *2*, 17–26.

39. Wen, D., Chen, G., Chen, Q., Li, P.Y., Cheng, H., and Gu, Z. (2019). Engineering protein delivery depots for cancer immunotherapy. Bioconjug. Chem. *30*, 515–524.

40. Desai, M.A., Webb, H.D., Sinanan, L.M., Scarsdale, J.N., Walavalkar, N.M., Ginder, G.D., and Williams, D.C., Jr. (2015). An intrinsically disordered region of methyl-CpG binding domain protein 2 (MBD2) recruits the histone deacetylase core of the NuRD complex. Nucleic Acids Res. *43*, 3100–3113.

41. Liu, Z., Fan, A.C., Rakhra, K., Sherlock, S., Goodwin, A., Chen, X., Yang, Q., Felsher, D.W., and Dai, H. (2009). Supramolecular stacking of doxorubicin on carbon nanotubes for in vivo cancer therapy. Angew. Chem. Int. Ed. *48*, 7668–7672.

42. Fuentes-Mattei, E., Velazquez-Torres, G., Phan, L., Zhang, F., Chou, P.C., Shin, J.H., Choi, H.H., Chen, J.S., Zhao, R., Chen, J., et al. (2014). Effects of obesity on transcriptomic changes and cancer hallmarks in estrogen receptor-positive breast cancer. J. Natl. Cancer Inst. *106*, https://doi.org/10.1093/jnci/dju158.

43. Wang, C., Wang, J., Zhang, X., Yu, S., Wen, D., Hu, Q., Ye, Y., Bomba, H., Hu, X., Liu, Z., et al. (2018). In situ formed reactive oxygen species-responsive scaffold with gemcitabine and checkpoint inhibitor for combination therapy. Sci. Transl. Med. *10*, https://doi.org/10.1126/scitranslmed.aan3682.

44. Stephan, S.B., Taber, A.M., Jileaeva, I., Pegues, E.P., Sentman, C.L., and Stephan, M.T. (2015). Biopolymer implants enhance the efficacy of adoptive T-cell therapy. Nat. Biotechnol. *33*, 97–101.